# WAVEFORM MODELING OF THE CRUST AND UPPER MANTLE USING S, SP, SSPMP, AND SHEAR-COUPLED PL WAVES FOR IMPROVED EVENT LOCATION, FOCAL DEPTH DETERMINATION, AND UNCERTAINTY ESTIMATION

Jay Pulliam and Mrinal K. Sen

University of Texas at Austin

Sponsored by Air Force Research Laboratory

Contract No. FA8718-04-C-0014

## ABSTRACT

During this contract's performance period (1 October 2004-30 September 2007) we intend to complete the development of a method for determining crust and upper mantle structure in aseismic regions and evaluate its capacity to produce sufficiently accurate models for locating hypocenters of small-to-moderate seismic events. Specifically, we will

- complete development of a waveform modeling approach to determine the structure of the crust and upper mantle in a broad region surrounding a broadband seismographic station;
- validate the method through careful comparison between models produced with our method and models produced by higher resolution active-source experiments, as well as models produced by surface wave inversion and receiver function methods;
- apply and validate methods for computing uncertainty statistics from the products of global optimization searches; and
- refine, apply, and evaluate waveform correlation methods to ground-truth data from regional events and explosions with well-constrained focal depths, using crust/upper mantle models produced with our method;
- apply the modeling method to teleseismic data recorded at stations in China, Africa, and the Middle East;
- apply and evaluate waveform correlation methods to determine focal depths for small- and moderate-magnitude regional events recorded at stations in China, Africa, and the Middle East using crust/upper mantle models determined in this study.

The high frequencies and long time-series required for phases that arrive near the direct SV phase, including Sp, SsPmP, and shear-coupled PL waves, their deep penetration into the Earth and observation at teleseismic distances make the computation of synthetic seismograms time-consuming. We have parallelized and optimized a synthetic seismogram code based on the reflectivity method and are now able to compute complete seismograms up to 0.5 Hz in just over one minute using eight AMD Opteron processors. This has allowed us to produce the best-fitting waveform matches that result from searches of many thousands of models, yet searching the model space comprehensively multiple times, as is required to estimate posterior covariance, correlation, and posterior probability distribution functions is still prohibitive. However, the speed-up in computation time is nearly linear with the number of processors used, so a massively parallel computer installed recently at the University of Texas at Austin should allow us to compute posterior probability density function (PPD) estimates readily. We intend to explore the utility of PPD estimates for estimating the reliability of our crustal models for the purposes of estimating hypocenters of small- to moderate-sized regional seismic events.

## OBJECTIVES

Our research focuses on developing and testing methods for determining event locations at regional distances (100-1,000 km) using one or a few three-component, broadband seismographic stations. To be useful for discriminating explosions from earthquakes, focal depths must be determined accurately to within a few kilometers, yet the structure of the crust and upper mantle between the source and station strongly influences the arrival times and amplitudes of regional phases. Our first task, therefore, is to determine this structure. We will attempt to obtain a sufficiently accurate model of crustal structure beneath a given station by searching over a wide variety of crustal models to find the one whose synthetics best match the amplitudes and travel times of phases that arrive in the time window around the direct S phase, and which appear most strongly on the radial component seismogram. We use data from large-magnitude (6<Mb<7) deep events located at teleseismic distances for this purpose, for reasons discussed in detail below.

After structural models are in hand we propose to find focal depths by means of a waveform correlation technique. We will compute suites of synthetic seismograms for the candidate model corresponding to a given broadband station and, given data from small-magnitude regional events recorded at the same station, compute correlations between the suites of synthetic seismograms generated for a variety of distances and focal depths.

Case studies around the world, including application to "ground-truth" data in which focal depths are well-constrained, are required in order to determine the range of applicability and usefulness of our event location strategy. Small magnitude events (2<mb<4) are rarely recorded at more than a few stations in many parts of the world, yet identifying these events is essential to monitoring nuclear explosions effectively. Our objective, therefore, is to develop and test methods for distinguishing between explosions and natural events in sparsely-instrumented parts of the world. Our strategy is to estimate hypocenter locations for small- and moderate-magnitude events using one or a few single broadband, three-component stations. Focal depth is a particularly helpful discriminating characteristic, if determined reliably.

## HISTORICAL PERSPECTIVE

The problem of finding earthquake locations using only a single three-component station, or a very sparse network of stations, has received a great deal of attention. Some authors, recognizing the greater difficulty in constraining focal depths, have focused on estimating event epicenters and origin times (e.g., Magotra et al., 1987; Roberts et al., 1989; Kedrov and Ovtchinnikov, 1990; Kim and Wu, 1997). Others have attempted to estimate not only focal depths but focal mechanisms, as well, via waveform modeling of regional events (Jimenez et al., 1989; Fan and Wallace, 1991; Zhao and Helmberger, 1994; Walter, 1993; Zhu and Helmberger, 1996). Frohlich and Pulliam (1999) review efforts to locate earthquakes using a single three-component station in detail. In contrast, the problem of determining earthquake focal depths with one or a few stations has received far less attention, yet obtaining accurate estimates of focal depths is important to tectonic interpretations of seismicity, to understanding seismic hazard, and to seismic monitoring of underground nuclear tests (National Research Council, 1997). If a seismic event were known reliably to have occurred at a depth greater than a few kilometers, one could confidently categorize that event as an earthquake rather than an explosion.

The most common approaches to determining focal depths utilize travel times (e.g., Douglas, 1967), which must be picked for the major seismic phases and then back-projected by a nonlinear or bootstrapped linear algorithm. A great deal of effort has been devoted to methods for picking arrival times automatically (Roberts et al., 1989; Saari, 1991). While these methods have proven useful for moderate to large magnitude events at far-regional and teleseismic distances, particularly for events that are deeper than a few tens of kilometers, they are prone to picking errors. These picking errors become relatively more important and more problematic for location procedures when dealing with small magnitude and shallow events. Furthermore, shallow events have little time separation between the downgoing, direct body wave phases and the upgoing, reflected ("depth") phases that are most useful for constraining focal depth. One must use high-frequency data to have any hope of identifying and picking distinct arrivals for these phases, which again complicates the picking process and increases the likelihood that errors will contaminate the location process. In some parts of the world, small-magnitude and relatively shallow events observed at regional distances typically have emergent rather than impulsive first arrivals, which renders travel time picking even more prone to errors. Lastly, reliable estimates of both epicenters and focal depths using travel times require redundancy, i.e., at least several and preferably many recordings from stations that are well-distributed with respect to azimuth around the event. But the great majority of earthquakes are small-magnitude, shallow events, which are much more likely than large events to be recorded by just one or a few seismographic stations. Locating

these small events accurately can be most useful for discriminating between nuclear explosions and earthquakes and can contribute a great deal to understanding regional tectonics.

Waveform modeling offers the best hope for constraining small-magnitude, shallow seismic events at regional distances with sparse observations. Ideally one would be able to match, and thereby determine the origin of, the time and amplitude of each arriving wave. Such a match is an unrealistic goal, in general, due to approximations required for tractability in modeling algorithms, to an incorrect or inadequately precise understanding of the crust and upper mantle in most regions, and to poor constraints on focal mechanisms and source time functions. While approaches such as finite difference methods offer hope for accurate and computationally feasible three-dimensional (3D) modeling in the relatively near future, to be useful they will require far more precise and accurate velocity models than are currently available. Assuming that accurate 3D, or even 2D, modeling is currently out of reach, the question that arises is whether 1D modeling methods can be used in a strategy that minimizes the effects of laterally-varying structure and focal mechanism to constrain the focal depths of seismic events. Presenting and evaluating such a strategy are the goals of our research. Rather than matching direct and reflected pulse shapes, as do Goldstein and Dodge (1999) for larger-magnitude (mb>=4.5) and more distant events, we seek to match some gross characteristics, such as the relative arrival times of a series of waves, as well as possible.

**A strategy for producing 1D models that are sufficiently accurate to constrain focal depths of small events**

Phases that arrive near the direct SV phase, including Sp (converted at the base of the Moho), SsPmP, and shear-coupled PL (SPL) waves, collectively sample the Earth's crust and upper mantle at oblique angles and therefore have the potential to produce an accurate lateral average of structural properties than teleseismic P waves. SPL waves essentially mimic the propagation characteristics of regional PL phases, with the important difference that the number of events available for modeling is often greater for relatively aseismic regions, since sources are located at teleseismic distances. SPL waves are sensitive to crust and upper mantle structure, including seismic velocity gradients, Vp/Vs, impedance contrast across the Moho, and layer thicknesses.

The conventional S phase (Figure 1) is the initial, relatively sharp and pulse-like arrival that signals the beginning of a wavetrain with generally longer periods and normal dispersion. The particle motion associated with the S phase is rectilinear and all three components of motion are in phase. The dispersive wavetrain, that follows S, exhibits prograde elliptical particle motion that is confined to the vertical plane. Oliver (1961) named this wavetrain "shear-coupled PL" because it is analogous to the PL wavetrain, which appears between P and S arrivals at regional distances. Oliver (1961) presented a theory, based on the observed group and phase velocity of SPL that explained the phase as coupling between S and the fundamental leaking mode of Rayleigh waves in the crustal waveguide. According to this theory, shear energy generated by an earthquake (or explosion) travels through the Earth's mantle as a body wave, whereupon it impinges upon the Moho. Afterward a portion travels through the crustal waveguide as trapped P-waves and leaky SV-waves (Figure 2). The only difference between a PL phase, which is observed at regional distances from a source, and SPL phases, which are observed at teleseismic distances, is that SPL is generated by a shear wave impinging upon the Moho at regional distances from the observing station. In addition to producing SPL as it impinges on the Moho, a portion of the incident S wave converts to P as well, which then travels through the crust to arrive at the station as a precursor to S (Figures 1 and 3). This phase is called Sp, and it has been used to model the crust by Jordan and Frazer (1975). Its sampling is much more localized to the station than is SPL's, making its sensitivity less representative of the broader region and more similar to that of P-coda receiver functions. SsPmP arrives at the base of the crust as a shear wave, travels upward through the crust as a shear wave, converts to a P wave at its surface reflection and bounces once off the Moho as a P wave. Langston (1996), while demonstrating that it can be highly useful for regional crustal modeling, showed that SsPmP can arrive before or after direct S, with either larger or smaller amplitude, and can also distort the S arrival pulse. We will attempt to simultaneously model S, Sp, and SsPmP that essentially isolates differences to the P structure of the crust, for data collected for SPL modeling. Because receiver function methods typically deconvolve the vertical seismogram, which is most sensitive to compressional wave energy, from the radial seismogram, constraints on P velocity are essentially sacrificed in order to obtain clean records of shear phases. The

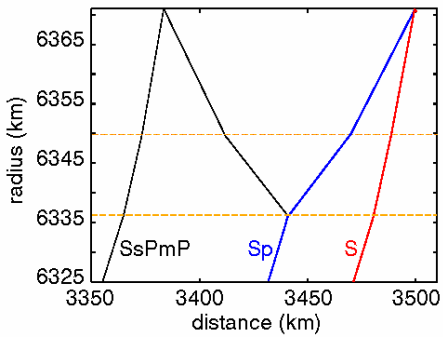


**Figure 1. Typical raypaths for S, Sp, and SsPmP. These body wave phases provide constraints on crustal thickness, P and S velocities near the station.**

data we propose to model will provide a valuable check of receiver functions, in that they constrain the bulk properties of the crust—average P velocity and crustal thickness (Sp and SsPmP)—and upper mantle (SPL). If the broad model search turns out to be too time-consuming or impractical, a fall-back strategy would be to first obtain a basic starting model by modeling Sp and SsPmP, then automating the SPL modeling using the Sp/SsPmP model as a starting point. Since reflectivity is a full-waveform method, there is no need to specify which phases should be included (nor need we identify or "pick" specific arrivals) in the waveform fitting procedure. While the waveform fitting itself will be automated, a great deal of exploration will be required to determine optimal window lengths, frequency content, and, perhaps, variable weighting functions for different portions of the seismograms.

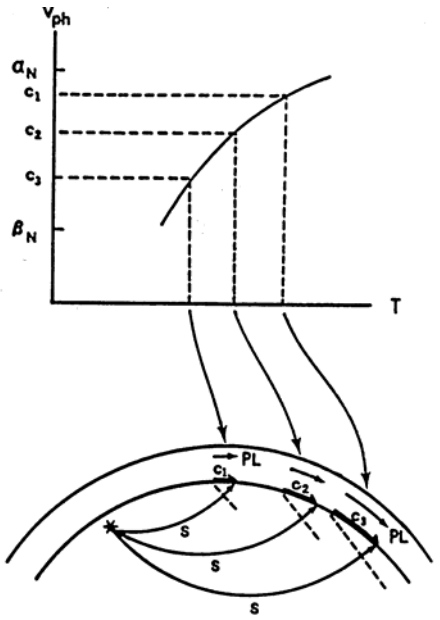


Excitation of *SPL*-waves with distance and corresponding period–phase velocity curve. $\alpha_N$, $\beta_N$: velocities of *P*- and *S*-waves at the Moho, *T*: period, $V_{ph}$: phase velocity.

**Figure 2. Propagation characteristics of shear-coupled PL phases (from Baag and Langston, 1985). Note that the distance of propagation of SPL, and therefore its sampling, depends on characteristics of the velocity structure, including the slope of velocities below the Moho and attenuation. The earliest-arriving and largest-amplitude SPL waves are those that have converted from S nearest to the station, so our modeling will weight local sampling more highly than distant sampling but the wavefield still averages structure laterally.**

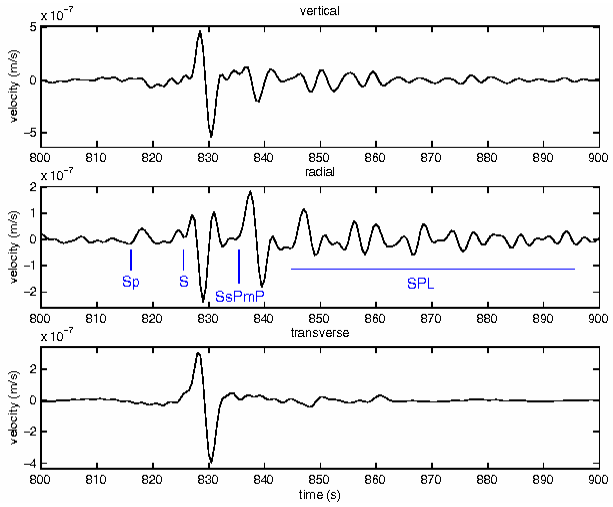


**Figure 3. Depending on Earth structure and an earthquake's radiation pattern, the phases Sp, S, SsPmP, and SPL may appear prominently on the radial component seismogram at distances between 30° and 75°.**

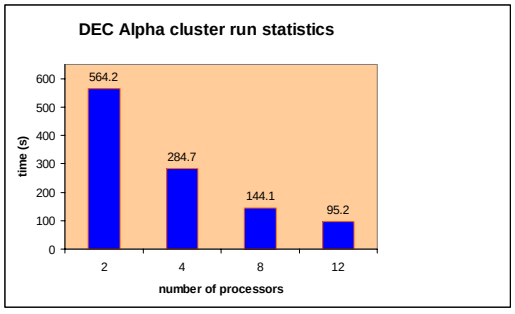


**Figure 4. Statistics of an example run to compute complete seismograms for frequencies from 0 to 0.5 Hz (number of frequencies = 2000, number of layers=192, number of ray-parameters=1000) on the DEC Alpha cluster. Note the near linear speedup of the algorithm with the increase in the number of processors.**

We are evaluating the usefulness of S, Sp, SsPmP (Figures 1 and 3), and shear-coupled PL (SPL) phases (Figures 2 and 3) for modeling crustal and upper mantle structure using real and synthetic data, developing a waveform inversion technique based on a novel implementation of the reflectivity method and global optimization algorithms, and applying this method to data recorded in China. We have made substantial progress in speeding up the synthetic seismogram computations to the point where a global optimization is feasible. The reflectivity calculation involves computation of reflectivity matrices for a stack of layers as a function of ray parameter (or wavenumber) and frequency. The computation of reflectivity responses for different ray parameters and frequencies are completely independent of each other. We took advantage of this independence to develop a reflectivity code that runs on parallel computer architectures. Our code loops over ray parameters, i.e., to each node we assign a certain number of ray parameters to compute. At the end, the master node assembles the partial responses and performs the inverse transformation to generate synthetic seismograms at the required azimuths and distances. We used MPI for message passing and ran our code on a PC cluster consisting of 16 nodes; each node is a 660MHz alpha processor with 8MB cache and 1GB of RAM. A Myrinet interconnect is used to communicate between nodes.

Figure 3 shows synthetic seismograms computed using our parallelized reflectivity code for a distance of 50° and an earthquake at 600 km focal depth. Since the reflectivity algorithm is "embarrassingly parallel" in that the response for each frequency or ray parameter can be computed on independent processors, without communication between processors, on a parallel machine computation speed increases nearly linearly with the number of processors (Figure 4). In a side-by-side comparison for various distances, source depths, and model complexity, our code matched results of the Fuchs-Muller code very well.

Our modeling method retains the time and cost advantages of P-coda receiver function methods but which uses types of data that are more appropriate for nuclear monitoring purposes: Shear-coupled PL phases (SPL), Sp phases converted at the Moho, and SsPmP. SPL samples the crust and upper mantle in the vicinity of a station most broadly compared to Sp, SsPmP and P and it emulates the propagation of regional phases, which reflect at more oblique angles (or are refracted by these layers) than are the more steeply arriving body phases typically used in receiver function modeling. In short, because of the data they use, the models produced by receiver function methods may be inadequate for the purposes of nuclear monitoring. These latter phases sample only a narrow cone beneath the station (e.g., Zhao and Frohlich, 1996). Modeled simultaneously (where they exist), SPL, Sp, and SsPmP offer the potential for producing azimuthally-dependent structural models.

We are pursuing this strategy because efforts to determine the locations of small, regional seismic events are hampered, in most parts of the world, by insufficient knowledge of the crust and upper mantle. Also, while focal depths are often a highly useful discriminant between explosions and earthquakes, their determination is quite sensitive to crustal structure. The most encouraging approaches to determining focal depths require precise modeling of seismic waveforms, particularly for small-magnitude events, in which travel time picks are relatively more prone to errors than for larger events. Yet, a precise modeling of waveforms at regional distances requires an accurate model of the crust and upper mantle along the propagation path between source and receiver.

## RESEARCH ACCOMPLISHED

### Forward Modeling

In order to explore the sensitivity of each phase we computed synthetics for a variety of distances using different crust and upper mantle models, including PREM (Dziewonski and Anderson, 1981), SNA (Grand and Helmberger, 1986), TNA (Grand and Helmberger, 1986), ECH (Zhao et al., 1991), and WCH (Beckers et al., 1999). Differences between these results point to sensitivity on the parts of these phases to distinct parts of the models' structure. Figure 5 shows an expanded comparison of waveforms produced using the different models for a single epicentral distance.

Figure 6 shows differences in waveform features to be expected from structural variations within China alone. The models at upper right were produced by Mangino et al. (1999) by modeling receiver functions for structure beneath stations of the China Digital Seismographic Network. The models differ primarily in the lower crust. One can see from the synthetics at left that these model differences are reflected by differences in the S coda, largely in SsPmP and SPL, for the distance range 30°-50°. These synthetics were produced for a 600-km deep event. This suggests that the relative timing of SsPmP-S and the phase and amplitudes of SPL phases are sensitive to the lower crust.

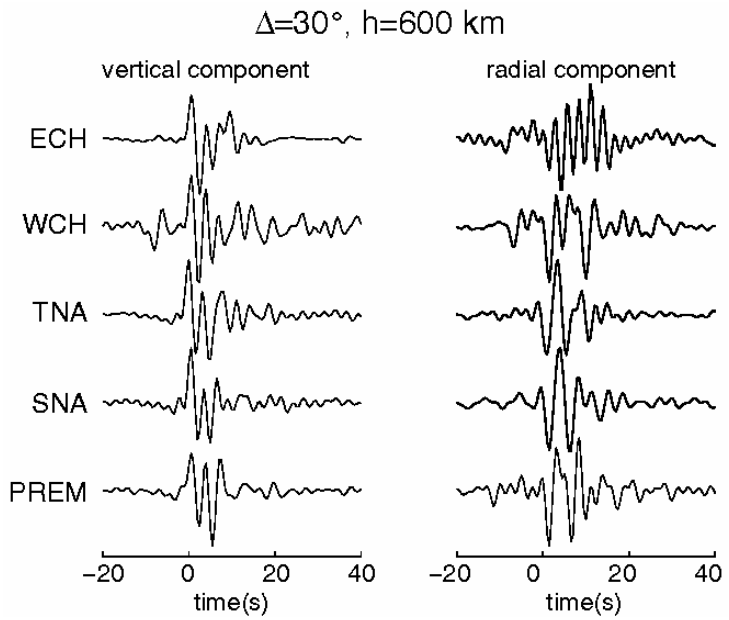


**Figure 5. Comparison of synthetic seismograms computed using various Earth models for the same deep, double-couple source at an epicentral distance of 30°. Differences in the arrival times and amplitudes of S, Sp, SsPmP and SPL indicate those phases' sensitivity to structure near the receiver.**

**Inverse Modeling**

Our modeling process is controlled by a global optimization algorithm called Very Fast Simulated Annealing (VFSA) (e.g., Sen and Stoffa, 1995). Simulated annealing (SA) is analogous to the natural process of crystal annealing when a liquid gradually cools to a solid state. The SA technique starts with an initial model $m_0$, with associated error or energy $E(m_0)$. It draws a new model $m_{new}$ from a flat distribution of models within the predefined limits. The associated energy $E(m_{new})$ is then computed and compared against $E(m_0)$. If the energy of the new state is less than the energy of the initial state, the new model is accepted and it replaces the initial model. However, if the energy of the new state is higher than the initial state, $m_{new}$ is accepted with the probability of $\exp\left(\left(E(\mathbf{m}_{new})-E(\mathbf{m}_0)\right)/T\right)$, where T is a control parameter called temperature. This rule of probabilistic acceptance (called the Metropolis rule) allows SA to escape local minima. The process of model generation and acceptance is repeated a large number of times with the annealing temperature gradually decreasing according to a predefined cooling schedule. A variant of SA, called Very Fast Simulated Annealing (VFSA) speeds up the annealing process by drawing new models from a temperature dependent Cauchy-like distribution centered on the current model. This change with respect to SA has two fundamental effects. First, it allows for larger sampling of the model space at the early stages of the inversion (when "temperature" is high), and much narrower sampling in the model space as the inversion converges and the temperature decreases, while still allowing the search to escape from local minima. Second, each model parameter can have its own cooling schedule and model-space sampling scheme. VFSA therefore allows for individual control of each parameter and the incorporation of a priori information. The model is parameterized in terms of layers, in which Vp, Vs, density, and layer thickness are free parameters.

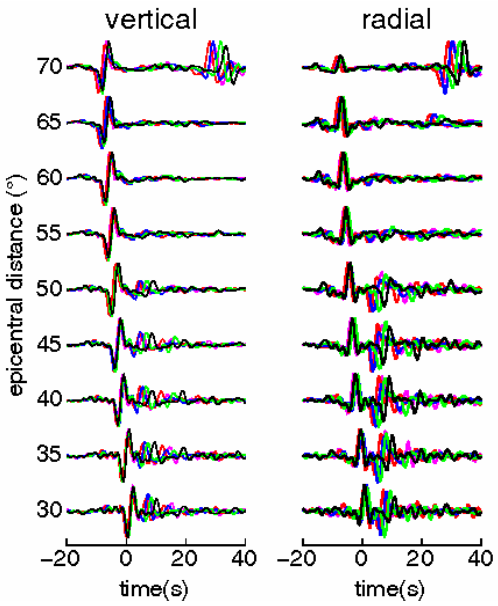


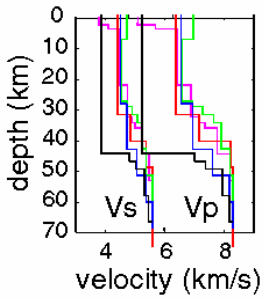


**Figure 6. Synthetic seismograms computed for various receiver function models of the crust and upper mantle beneath China (models from Mangino et al., 1999). The primary differences between the seismograms are in the S coda, including SsPmP and SPL, which indicates these phases are highly sensitive to distinguishing structural details of these models.**

In seismic inversion, more than one model can often explain the observed data equally well and trade-offs between different model parameters are common. It is therefore important not only to find a single, best-fitting solution but also to find the uncertainty and level of uniqueness of that solution. A convenient way to address these issues is to cast the inverse problem in a Bayesian framework (e.g., Tarantola, 1987; Sen and Stoffa, 1995) in which the posterior probability density function (PPD) is the answer to the inverse problem. "Importance sampling" based on a Gibbs sampler or a Metropolis rule (Sen and Stoffa, 1998) can be used effectively to evaluate the necessary multi-dimensional integrals and to estimate PPD, posterior mean, covariance and correlation matrices. The posterior covariance and correlation matrices quantify the trade-off between different model parameters. Sen and Stoffa (1995) showed that multiple VFSA runs with different random starting models could be used to sample models from the most significant parts of the model space. This "poor man's" importance sampling, which is computationally efficient, results in estimates that are fairly close to the values obtained by theoretically-correct Gibbs sampling.

**Example of an Application to Data from the China Digital Seismographic Network**

Figure 7 shows the result of modeling radial and vertical records from station BJT of the 9/28/1994 event in Indonesian. Subjective choices must be made in the modeling about which parts of the seismogram to try to fit. In regions with strong lateral variations or anisotropy, it may be that no single 1D model will predict all the phases adequately. Requiring the modeling to try to fit each phase similarly will result in a model that does not predict any single phase well. Given the sampling produced by the various phases, we tried to prioritize fits in the following order: SPL, SsPmP, SV, and Sp. Given the broad sampling and lateral averaging performed by SPL we believe that the single 1D model that fits SPL best will be the most useful for locating earthquakes regionally. SsPmP also has a broad sample and constrains Vp, so it's second in priority. This priority order reflects a starting point—an initial preference—and will be evaluated as a strategy.

To implement this strategy we successively try to fit broader time windows of the data waveforms. 8 15 shows the results of 600 iterations in which only the window between 815 s and 860 s is evaluated for correlation at each iteration. The BJT receiver function model of Mangino et al. (1999) is shown for comparison, although it is not a "reference" or "starting" model in any sense. In our procedure we specify the search limits (also shown in Figure 8) and the first candidate model is chosen randomly. Figure 9 shows an attempt to fit a broader window that includes SV and Sp. Differences between the two final models shown in Figures 7 and 8 are again concentrated in the lower crust, between 30 and 50 km depth. Figure 9 shows the result of a 600-iteration run to model records from BJT of the 11/15/1994 Indonesia event, in which the time interval fit is restricted to include SsPmP and SPL. Figure 10 shows the results of a 600-iteration run to fit a broader window, as in Figure 8. Figure 11 shows results for a third event, also recorded at BJT. Figure 12 compares the models produced for the region containing BJT with Mangino et al.'s (1999) receiver function model, in the context of the imposed search limits.

## CONCLUSIONS AND RECOMMENDATIONS

For the optimization example shown in Figure 8, depth zones A, B, and C in Figure 13 correspond to parameter correlations indicated by the same labels in Figure 14. Note that the thin, shallow layers in A are characterized by significant off-diagonal cross-correlations (trade-offs) with other parameters. This indicates that the data do not constrain these layers well. Also, the symmetric "variances" about the mean (actually 1 standard deviation) do not contain the best-fitting model at this depth, pointing to the non-linearity of the inverse problem. We defined the prior to be Gaussian, so the computed (posterior) variances are also symmetric, but the fact that the best-fitting model lies outside this distribution suggests that the true distribution is skewed. Zone B, in contrast, contains a low-velocity zone in Vs that appears to be well-constrained (Figure 13). There is no corresponding Vp low-velocity zone.

Results for Zone C suggest that the data do not place strong constraints on the model parameters at these depths, on the one hand. However, since the best-fitting model is pegged against the search limits for both Vp and Vs, we will widen the search limits and perform a greater number of VFSA iterations to explore this zone further.

## REFERENCES

Baag, C.-E. and C.A. Langston, Shear-coupled PL, *Geophys. J. R. Astr. Soc.,* 80, 363-385, 1985.

Beckers, J., S. Schwartz, and T. Lay, *Geophys. J. Int.*, 119, 574-594, 1994

Douglas, A. (1967). Joint hypocentral determination, *Nature*, 214, 47-48.

Dziewonski, A. M., Anderson, D. L., Preliminary reference Earth model, *Phys. Earth. Planet. Int.,* 25, p. 297-356, 1981.

Fan, G. and T. Wallace (1991). The determination of source parameters for small earthquakes from a single, very broadband seismic station, *Geophys. Res. Lett.,* 18, 1385-1388.

Frazer, L.N., Synthesis of shear coupled PL. *Ph.D. thesis*, Princeton University, 54 pp., 1977.

Frohlich, C., and J. Pulliam (1999). Single-station location of seismic events: A review, and a plea for more research, *Phys. Earth Planet. Int.*, 113, 277-291.

Goldstein, P., and D. Dodge (1999). Fast and accurate depth and source mechanism estimation using P-waveform modeling: A tool for special event analysis, event screening, and regional calibration, *Geophys. Res. Lett.,* 26, 2569-2572.

Grand, S.P., and D. Helmberger, Upper mantle shear structure of North America, Geophys*. J. R. Astr. Soc.,* 76, 399-438, 1984

Jimenez, E., M. Cara, and D. Rouland (1989). Focal mechanisms of moderate-size earthquakes from the analysis of single-station three-component surface-wave records, *Bull. Seism. Am.,* 79, 955-972.

Jordan, T.H., and L.N. Frazer, Crustal and upper mantle structure from Sp phases, J. Geophys. Res., 80, 1504-1518, 1975.

Kedrov, O.K., and V.M Ovtchinnikov (1990). An on-line analysis system for three-component seismic data: Method and preliminary results, *Bull. Seism. Am.,* 80, 2053-2071.

Kim, S. G. and Z. Wu (1997). Uncertainties of seismic source determination using a 3-component single station, *J. Phys. Earth*, 45, 1-11.

Langston, C.A., The SsPmP phase in regional wave propagation, *Bull. Seism. Soc. Am*., 86, 133-143, 1996.

Magotra, N., N. Ahmed and E. Chael (1987). Seismic event detection and source location using single-station (three-component) data, *Bull. Seism. Soc. Am.,* 77, 958-971.

Mangino, S., K. Priestley, and J. Ebel, The receiver structure beneath the China Digital Seismograph Network Station, *Bull. Seism. Soc. Am.,* 89, 1053-1076, 1999

National Research Council (1997). Research Required to Support Comprehensive Nuclear Test Ban Treaty Monitoring, National Academy Press, Washington, D. C., 139 pp.

Oliver, J., On the long period character of shear waves, *Bull. Seism. Soc. Am.*, 51, 1-12,1961.

Roberts, R. G., A. Christoffersson and F. Cassidy (1989). Real-time event detection, phase identification and source location estimation using single-station three-component seismic data, *Geophys. J.,* 97, 471-480.

Saari, J. (1991). Automated phase picker and source location algorithm for local distances using a single three-component seismic station, *Tectonophysics*, 189, 307-315.

Sen, M., and P. L. Stoffa, 1995, Global Optimization Methods in Geophysical Inversion, Elsevier Science Publishing Company, The Netherlands.

Tarantola, A., Inverse Problem Theory: Methods for Data Fitting and Model Parameter Estimation, 613 pp., Elsevier, Amsterdam, 1987.

Walter, W. R. (1993). Source parameters of the June 29, 1992 Little Skull Mountain earthquake from complete regional waveforms at a single station, *Geophys. Res. Lett*., 20, p. 403-406.

Zhao, L.-S., D. Helmberger, and D.V. Harkrider, *Geophys. J. Int.*, 105, 713-730, 1991.

Zhao, L.-S. and C. Frohlich. Teleseismic body waveforms and receiver structures beneath seismic stations, *Geophys. J. Int.,* 124, 525-540, 1996.

Zhu, L. and D.V. Helmberger (1996). Advancement in source estimation techniques using broadband regional seismograms, *Bull. Seism. Soc. Am.,* 86, 1634-1641.

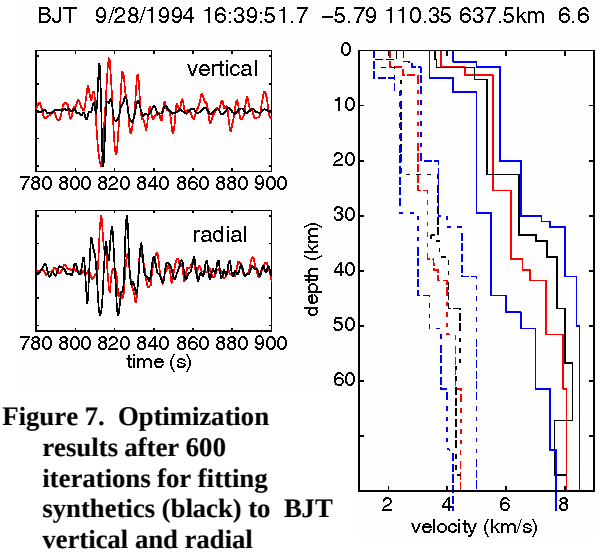


**Figure 7. Optimization results after 600 iterations for fitting synthetics (black) to BJT vertical and radial records (red) of the 9/28/1994 event, using the time interval 815-860 s. Best-fitting model (black), search bounds (blue), and receiver function model by Mangino et al. (1999)**

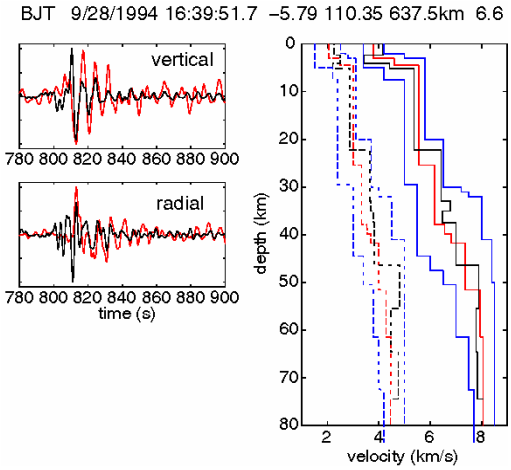


**Figure 8. Same as in Figure 7 except that the interval 800-860 s was used in the waveform fitting.**

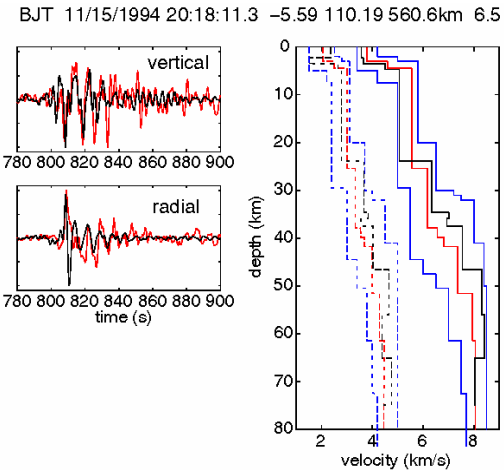


**Figure 10. Same as in Figure 9 except that the interval 800-860 s was used in the waveform fitting.**

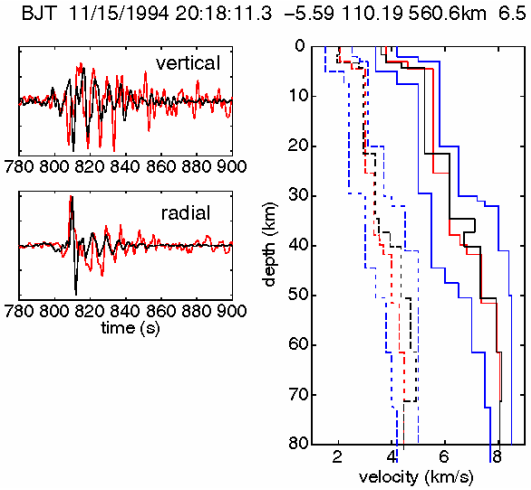


**Figure 9. Optimization results after 600 iterations for fitting synthetics (black) to BJT vertical and radial records (red) of the 11/15/1994 event, using the time interval 815-860 s. Best-fitting model (black), search bounds (blue), and receiver function model by Mangino et al. (1999) (red).**

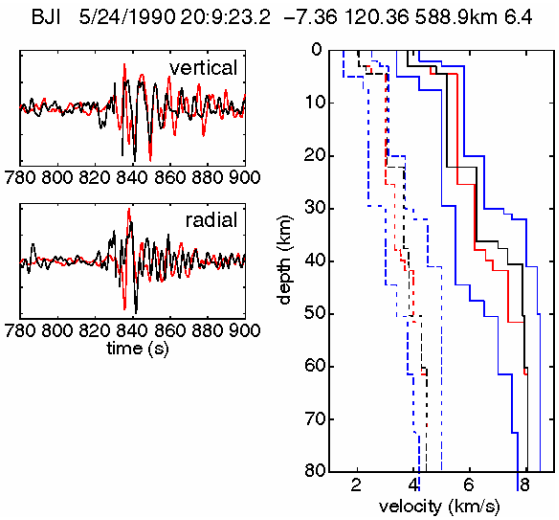


**Figure 11. Optimization results after 400 iterations for fitting synthetics (black) to BJT vertical and radial records (red) of the 5/24/1994 event, using the time interval 835-870 s. See Figure 9 for other details.**

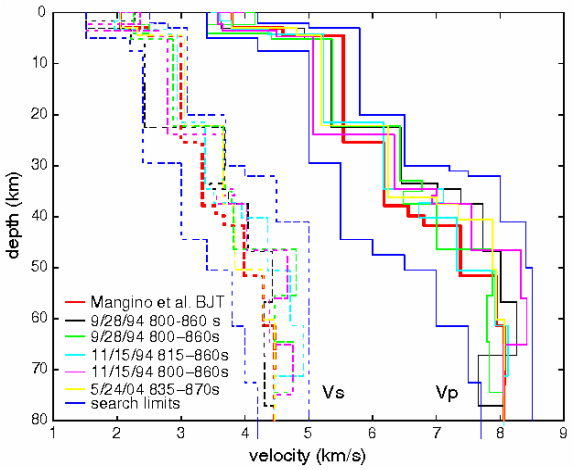


**Figure 12. Comparison of models for the crust and upper mantle in the vicinity of station BJT resulting from waveform fits to various data (see legend), Mangino et al.'s (1999) receiver function model (red), and the simulated annealing search limits (blue).**

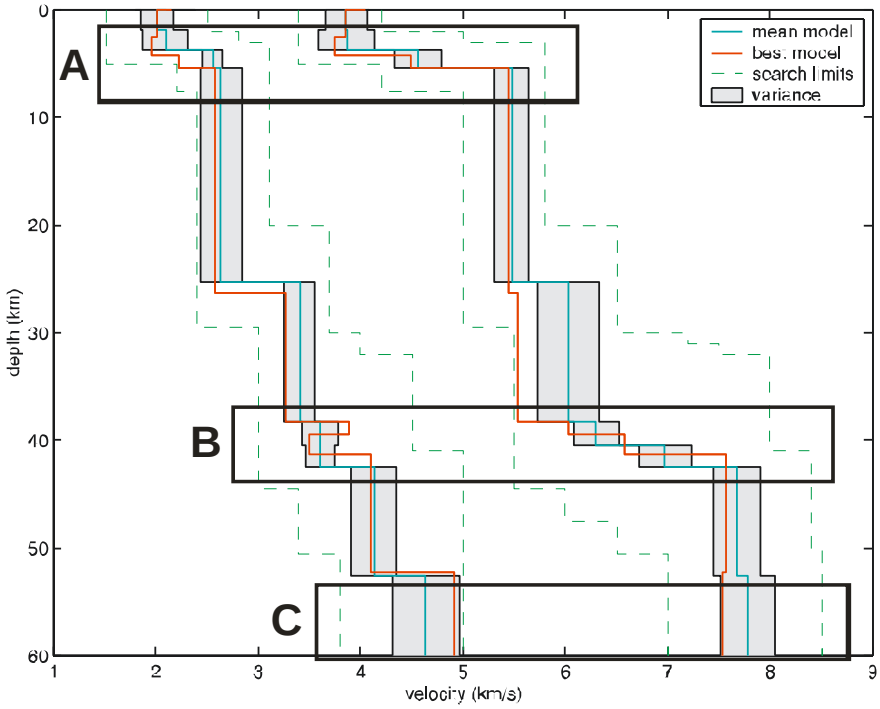


**Figure 13. Mean (cyan) and best-fitting (red) models and variance of the optimization run shown in Figure 8. Search limits imposed by the operator at the outset are shown in green. Variances are only shown for Vs (left) and Vp (right).**

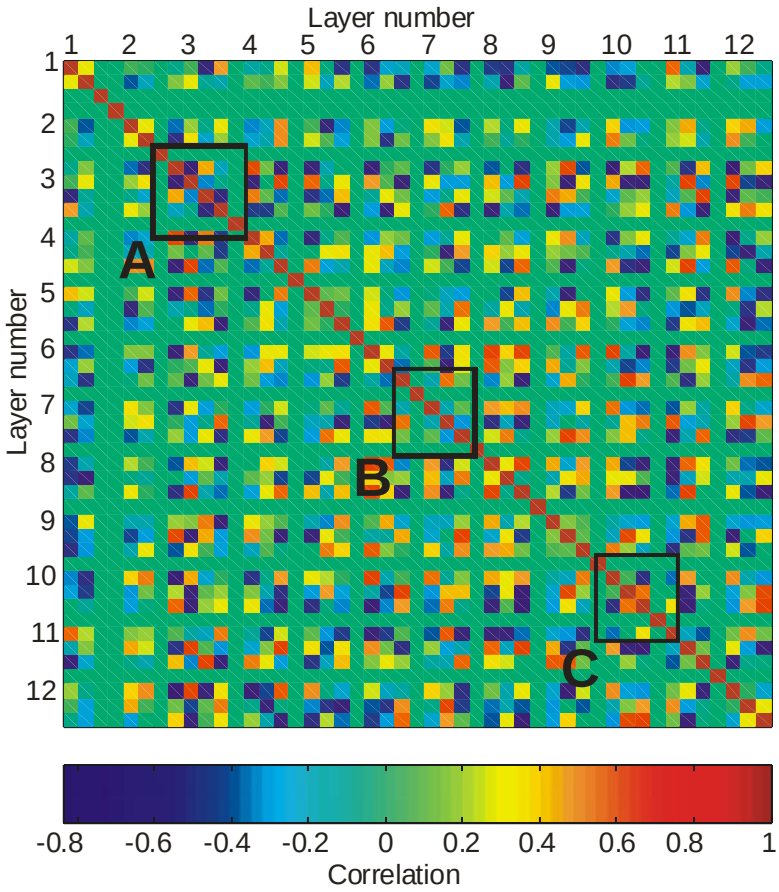


**Figure 14. Parameter correlations computed for the optimization run shown in Figure 15. There are four independent parameters: Vp, Vs, layer thickness, and density, repeated in that order for 12 layers. The total of 48 parameters is shown here in color (left) and with a modified grayscale, in which zero correlation is white and perfect positive and negative correlations are both black (right).**